



**HAL**  
open science

## Identification of an amorphous-amorphous two-step transformation in indomethacin embedded within mesoporous silica

B. Malfait, Laurent Paccou, Natalia T. Correia, Yannick Guinet, Alain Hedoux

### ► To cite this version:

B. Malfait, Laurent Paccou, Natalia T. Correia, Yannick Guinet, Alain Hedoux. Identification of an amorphous-amorphous two-step transformation in indomethacin embedded within mesoporous silica. *Microporous and Mesoporous Materials*, 2021, 328, pp.111502. 10.1016/j.micromeso.2021.111502 . hal-03464481

**HAL Id: hal-03464481**

**<https://hal.science/hal-03464481>**

Submitted on 5 Jan 2024

**HAL** is a multi-disciplinary open access archive for the deposit and dissemination of scientific research documents, whether they are published or not. The documents may come from teaching and research institutions in France or abroad, or from public or private research centers.

L'archive ouverte pluridisciplinaire **HAL**, est destinée au dépôt et à la diffusion de documents scientifiques de niveau recherche, publiés ou non, émanant des établissements d'enseignement et de recherche français ou étrangers, des laboratoires publics ou privés.



Distributed under a Creative Commons Attribution - NonCommercial 4.0 International License

## **Identification of an amorphous-amorphous two-step transformation in indomethacin embedded within mesoporous silica**

Benjamin Malfait<sup>1,2</sup>, Laurent Paccou<sup>2</sup>, Natalia T. Correia<sup>2</sup>, Yannick Guinet<sup>2</sup>, and Alain Hedoux<sup>2\*</sup>

<sup>1</sup>Institute of Physics of Rennes, CNRS-University of Rennes 1, UMR 6251, F-35042 Rennes, France

<sup>2</sup>Univ. Lille, CNRS, INRAE, Centrale Lille, UMR 8207 - UMET - Unité Matériaux et Transformations, F-59000 Lille, France

\*corresponding author : [alain.hedoux@univ-lille.fr](mailto:alain.hedoux@univ-lille.fr)

### Abstract

A very unusual amorphous-amorphous two-step transformation was observed in indomethacin confined within MCM-41 mesoporous silica, via isothermal and non-isothermal routes. Isothermally, at room temperature, the first step corresponds to the 1-dimensional growth of  $\gamma$ -nanocrystals along the mesoporous channels from preexisting incipient nuclei. In the second step nanocrystals slowly transform into an undercooled liquid state structurally different from the original liquid and characterized by a higher molecular mobility. The instability of nanocrystals detected in the continuation of the isothermal growth was explained as resulting from a very high specific area of nanocrystals imposed by the geometrical confinement when the size of nanocrystals along the channels achieves a dimension much larger than the channel diameter. The mechanism of the slow dissolution of nanocrystals was identified as similar to a digestive ripening process, inverse to the Ostwald ripening, by which larger clusters dissolve to the detriment of smaller ones. This two-step transformation was also observed upon heating. In this case, the growth of nanocrystals is followed by a melting far below the melting point of  $\gamma$ -crystals, according to Gibbs-Thomson effects. This study shows that the original amorphous form of indomethacin transforms into a second amorphous form via the transient growth of nanocrystals which become unstable via two different mechanisms induced by the geometrical confinement.

Keywords: geometrical confinement – nanocrystals stability – specific area – Raman spectroscopy – pharmaceuticals

## 1. Introduction

The existence of polyamorphism was reported for a number of organic molecular materials (triphenyl phosphite[1], n-butanol[2], mannitol[3]) and has been associated with a first-order phase transition detected below the melting point between the undercooled liquid and an apparently amorphous state structurally different from the original liquid state. This type of unconventional phase transformation, leading to the consideration of a second critical point or the existence of two distinct liquids widely implied in the emblematic case of water[4], is still a hotly debated subject nowadays[5-7]. It is worth noting that the polyamorphic transformation of the above mentioned organic molecular compounds was systematically associated with the detection of nanocrystals coexisting with the undercooled liquid along the devitrification process[8, 9]. Devitrification is mostly related to the lifetime of nanocrystals which strongly depends on the crystallite size, according to the Gibbs-Thomson equation. The phase transformation of a metastable undercooled liquid is controlled by three overlapping processes, namely nucleation, growth and eventually ripening. As nucleation and growth rates decrease, the interfacial effects (Gibbs-Thomson) become preponderant[10] and the smaller clusters dissolve transferring their mass to larger growing clusters. The transition from nucleation-and-growth to ripening is highly dependent on interfaces, including interface curvature and surface tension at the liquid-solid interface[11]. In this study the geometrical confinement of molecular materials in well-characterized ordered mesoporous silica is used to induce significant interfacial effects. Only a solid-state method of loading by milling[12] (milling-assisted loading, MAL, described in Supporting Information, SI Figure S1) gives the opportunity to analyze crystallization mechanism at the nanoscale from pre-existing nuclei, since nucleation is inhibited by spatial restrictions using conventional loading methods based on capillarity (either by melting or dissolving materials). Indeed, pioneering works have shown[13] the capability of manipulating the physical state of ibuprofen (from the amorphous state to a distribution of crystallites coexisting with undercooled liquid) within SBA-15 matrices by fine tuning of the channel size. The recent development of a solid-state loading method[12] by the authors[12] doesn't require molecular adsorption from the liquid state, and then makes possible crystallization bypassing nucleation[13]. This innovative MAL method was also used by other groups[14] unambiguously confirming its efficiency for loading molecular materials.

Here, MCM-41 was used as mesoporous silica matrix, in order to impose more severe surface effects than SBA-15 to the adsorbed molecular nano-organizations for subsequent analyzes. The distribution of pore size ( $D_p = 2.8$  nm) is plotted in Figure S2. The pharmaceutical area provides remarkable systems with rich polymorphism and atypical metastable situations that make them candidates as polyamorphic systems. Among active pharmaceutical ingredients (APIs), indomethacin (IMC) exhibits an original monotropic  $\alpha$ - $\gamma$  polymorphism in which the denser form ( $\alpha$ ) is metastable at room temperature[15]. Its glass transition temperature ( $T_g = 42$  °C)[16] is

slightly above room temperature, and then it cannot be amorphized outside the pores just by the milling effect at room temperature[17].

In the present study, we report the analysis of isothermal and non-isothermal transformations of IMC confined within MCM-41 using MAL method. IMC was loaded in MCM-41 matrices using conditions relatively far below the optimum conditions of filling (40 wt%), by co-milling IMC crystals (20 wt%  $\gamma$ -IMC) with MCM-41 (80 wt%) at 30 Hz for 30 minutes at room temperature, in order to ensure the total loading of IMC within the pores. Raman spectroscopy was used to analyze the physical state of confined IMC. It was previously shown that the C=O stretching region lying from 1500 to 1750  $\text{cm}^{-1}$  is distinctive of each form of IMC[18], and can be used for determining a degree of crystallization[19]. Spectra of the various forms of IMC are plotted in Figure S3. Additionally, low-wavenumber Raman spectroscopy gives the opportunity to analyze the molecular organization and the phase transitions in disordered molecular materials. Another considerable advantage of Raman spectroscopy for analyzing IMC confined in MCM-41 results from the quasi absence of Raman signal of the mesoporous silica matrices compared with the high intensity of Raman spectra of active pharmaceutical ingredients, rich in  $\pi$ -bonds which enhance the Raman polarisability[20]. The comparison of spectra of MCM-41 and  $\gamma$ -crystals in the bulk form collected in the same conditions especially same acquisition time is shown in Figure S4.

## 2. Materials and methods

### 2.1. Materials

Indomethacin (2-[1-(4-chlorobenzoyl)-5-methoxy-2-methylindol-3-yl]acetic acid), CAS number : 53-86-1, purity higher than 98.5% was purchased from Sigma-Aldrich and it was used without further purification. MCM-41, CAS number: 112-02-7, ( $S_{\text{BET}} = 1033 \text{ m}^2/\text{g}$ , total pore volume  $V_{\text{abs}} = 1.18 \text{ cm}^3/\text{g}$ , and pore size  $D_p = 3.6 \text{ nm}$ ) was purchased from Sigma-Aldrich. More information about MCM-41 including the distribution of the pore size are given in Supplementary Material (figure S2).

### 2.2. Experimental conditions for Raman spectroscopy investigations

**Raman spectra in the C=O stretching region** were collected using a Renishaw In Via micro-Raman spectrometer equipped with a 785 nm laser diode. An achromatic lens was used to focus the laser beam on the composite and to collect the  $180^\circ$  scattered light in order to analyze the largest possible volume of the sample. The sample temperature was regulated in a THMS 600 Linkam device for analyzing isothermal annealing at room temperature and heating ramps.

**Low-wavenumber Raman spectra** were collected using a high-resolution Raman XY-Dilor spectrometer to analyze the non-polarized back-scattered light. The spectrometer is composed of a double monochromator comprising four mirrors characterized by a focal length of 800 mm, and a spectrograph. The choice of experimental conditions (incident radiation, entrance and exit slit width opened at 200  $\mu\text{m}$ ) gives a spectral resolution of about  $1 \text{ cm}^{-1}$  in the 5 – 250  $\text{cm}^{-1}$  region,

and allows the rejection of exciting light (the 660 nm line of a solid diode laser) down to  $5\text{ cm}^{-1}$ . The spectrometer is equipped with a liquid nitrogen cooled charge coupled device detector. The high sensitivity of the detector and the large analyzed scattered volume ( $\sim 0.5\text{ cm}^3$ ) allow us to record low-wavenumber Raman spectra in the  $5 - 250\text{ cm}^{-1}$  range in 120 seconds. Powder samples were loaded in spherical pyrex cells hermetically sealed. The temperature of sample was regulated using an Oxford nitrogen flux device that keeps temperature fluctuations within  $0.1\text{ }^\circ\text{C}$ .

### 3. Results and discussion

**A first set of investigations** focuses on the isothermal behavior at room temperature of composites prepared by co-milling 20 wt% of IMC- $\gamma$  crystalline powder and MCM-41. Spectra were continuously collected with an acquisition time of 1 minute every minute for more than 8 hours. The first spectrum collected during the isothermal annealing at room temperature (RT) is plotted in Figure 1, is compared to the spectrum of the  $\gamma$ -crystalline polymorph, and to the spectrum of the glassy state in the bulk form. The spectrum of the composite shows the signature of the  $\gamma$  form, i.e. the sharp band around  $1700\text{ cm}^{-1}$  emerging from the broad band distinctive of the amorphous state.

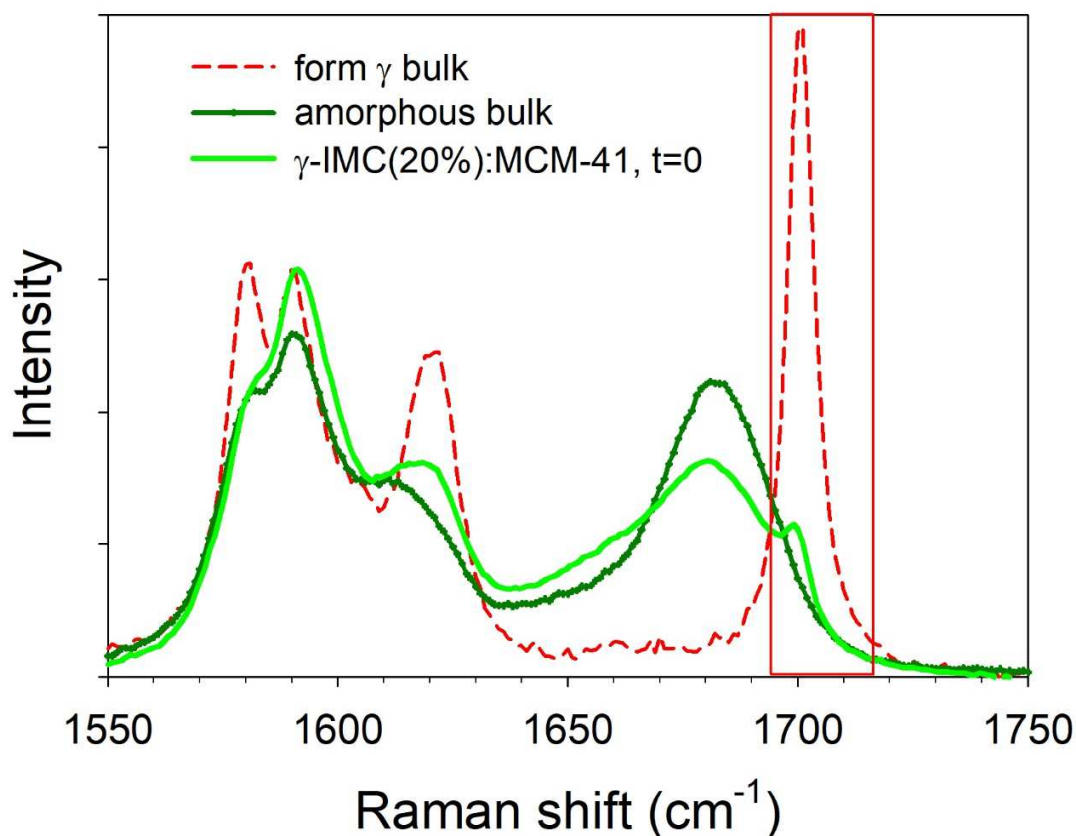


Figure 1. Raman spectrum of intramolecular C=O stretching region of amorphous IMC,  $\gamma$ -IMC in bulk form, and  $\gamma$ -IMC(20%):MCM-41 composite taken just after prepared by MAL method. The framed spectral zone was used for analyzing the physical state of confined IMC.

A fitting procedure described in Figure S5 was used for analyzing each spectrum taken during the isothermal annealing. The integrated intensity of the sharp emerging band at 1700 cm<sup>-1</sup> resulting from this fitting procedure compared to that obtained from fitting the spectrum of form  $\gamma$  provides a degree of crystallization, as described in Figure S5, estimated to 4% for the first spectrum collected in the freshly prepared composite. Figure 2 shows the time dependence of the spectrum of the composite for more than 10 hours (Figure 2a). It reveals the continuous intensity increase of the 1700 cm<sup>-1</sup>, corresponding to the crystal growth of  $\gamma$ -nanocrystals, stopping to a maximum of crystallinity slightly above 30%. Surprisingly, upon further isothermal annealing at RT (Figure 2b), the intensity of the 1700 cm<sup>-1</sup> band slowly decreases, reflecting the very slow transformation of nanocrystals into liquid. It is important to note that both the crystal growth and the disappearance of nanocrystals are not induced by energy transfer from the laser spot to the composite, considering the very low power measured at the level of the sample (~ 50 mW in the near infrared domain, 785 nm). The time dependence of the degree of crystallinity obtained from the integrated intensity of the 1700 cm<sup>-1</sup> band is plotted in Figure 2c. Given the long time of the complete isothermal transformation (more than 10 days), spectra cannot be collected continuously and the degree of crystallinity was plotted until a hundred hours. The first step of the isothermal annealing at RT corresponding to the growth of  $\gamma$ -nanocrystals was analyzed in the frame of the nucleation and growth theory. Experimental data plotted in the inset of Figure 2c were fitted with the following function according to the Kolmogorov-Johnson-Mehl-Avrami (KJMA) equation[21]:

$$[X(t) - X_{max}] \propto -\exp[-k(t)^n]$$

where  $X(t)$  represents the crystallized fraction at time  $t$ ,  $X_{max}$  the maximum crystallized fraction,  $k$  is a constant dependent on the nucleation and growth rate, and  $n$  is a parameter reflecting both the nucleation process ( $n=1$ ) and the dimension of the crystallization growth ( $n=1$  to 3 for 1 to 3-dimensional growth). The exponent was determined very close to 1 ( $0.98 \pm 0.02$ ), reflecting the absence of nucleation and the 1-dimensional growth. This result can be interpreted from the consideration of 1-dimensional growth along the channels of the MCM-41 matrix from preexisting  $\gamma$ -IMC incipient nuclei. In the first spectrum ( $t=0$ ) of the data collection, the detection of a shoulder on the high-frequency side of the broad band distinctive of the amorphous state in the bulk form indicates an instantaneous crystallization beginning during the preparation of the sample (~15 min).

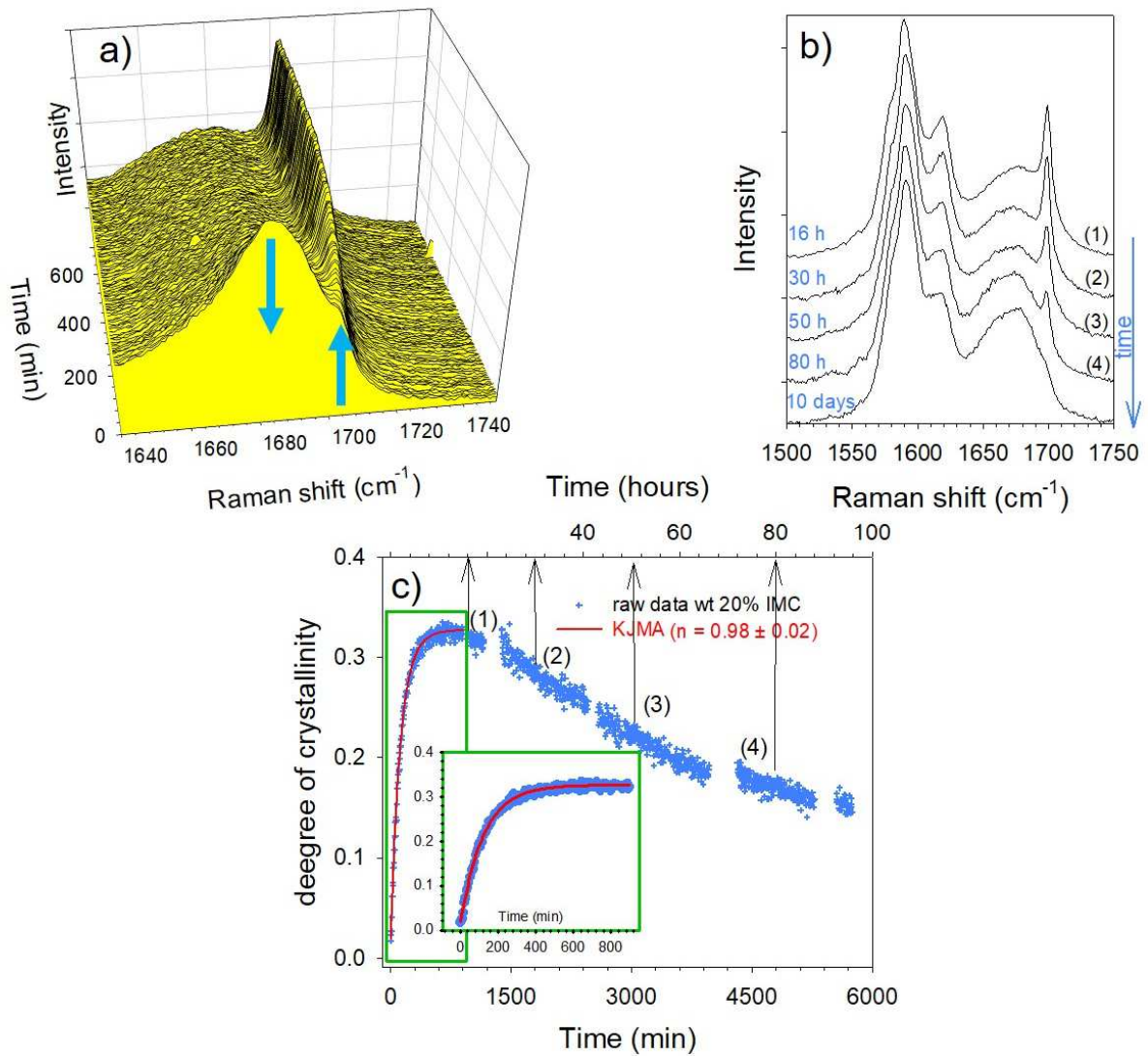


Figure 2. Isothermal aging of IMC confined in MCM-41 by MAL method; a) time dependence of the Raman C=O stretching spectrum of the  $\gamma$ -IMC(20%):MCM-41 composite in the first step of the transformation; b) in the second step, the spectrum numbering indicating the degree of the transformation in the complete kinetics; c) time dependence of the degree of crystallization of  $\gamma$ -IMC(20%):MCM-41 composite determined from the integrated intensity of the 1700  $\text{cm}^{-1}$  band, discontinuously analyzed for a hundred hours;

**A second set of experiments** was performed on heating composites obtained with the same conditions of loading, from 30 °C up to 120 °C at 0.5 °C/min. The C=O stretching spectrum was collected with the acquisition time of 60 s, every 0.5 °C. Spectra collected during the first heating ramp of the composite are plotted in Figure 3a in a narrower window from 1640 to 1720  $\text{cm}^{-1}$  to give a clear description of phenomena observed upon heating.

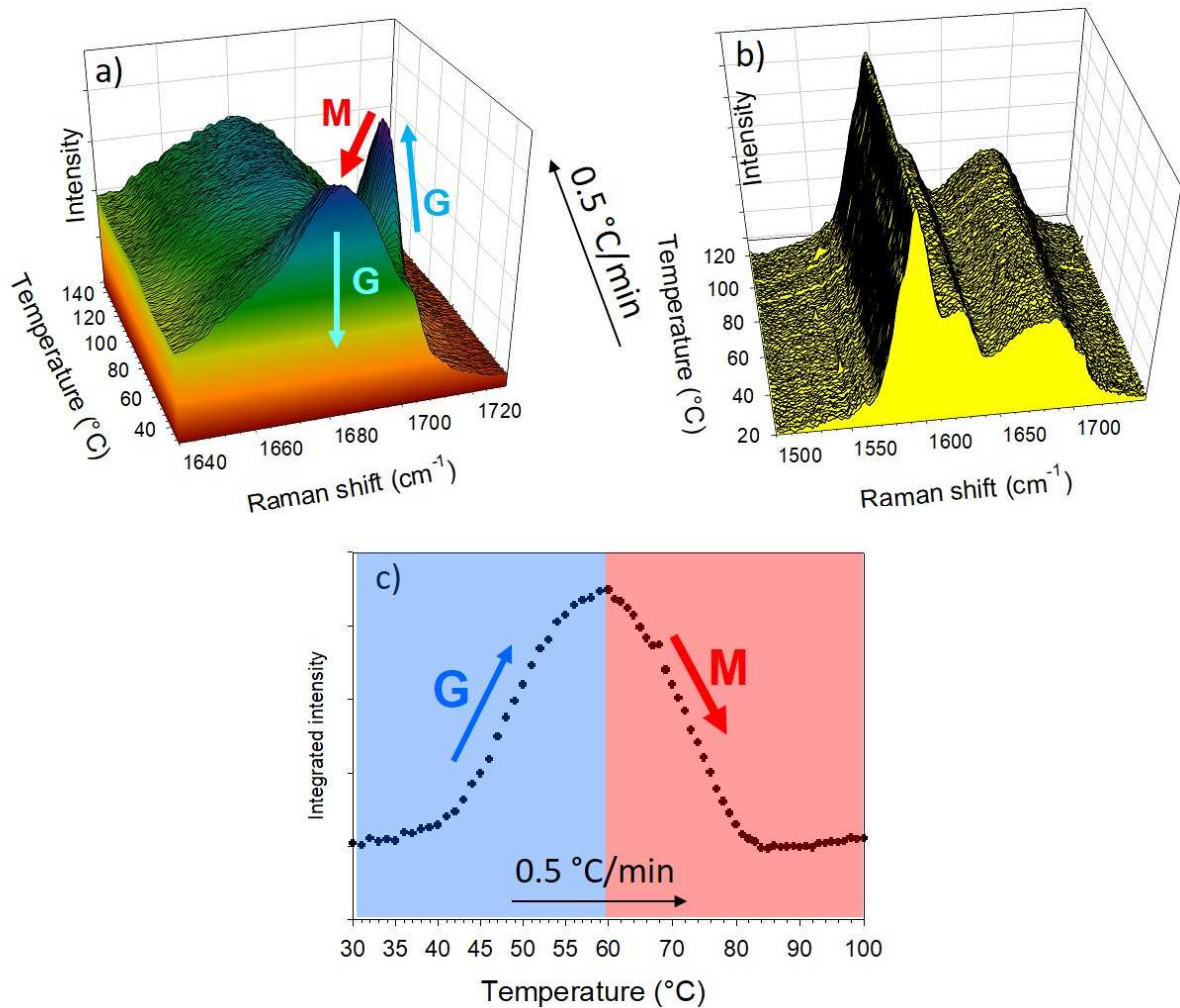


Figure 3. Analysis of confined IMC in MCM-41 upon heating:

- Temperature dependence of the Raman spectrum in the 1640 – 1750  $\text{cm}^{-1}$  region (for a better observation of the bands distinctive of the amorphous and  $\gamma$ -crystalline states) taken upon heating the composite at 0.5 °C/min; arrows indicate intensity changes observed along the growth of crystallites (G) and melting of crystallites (M)
- Temperature dependence of the spectrum in a more extended region; spectra are collected during a second heating ramp at 0.5 °C/min; no change was detected indicating the absence of crystallization
- Temperature dependence of the integrated intensity of the 1700  $\text{cm}^{-1}$  band determined for each spectrum collected upon heating the  $\gamma$ -IMC(20%):MCM-41 composite

The integrated intensity of the  $1700\text{ cm}^{-1}$  band, considered as proportional to the crystallization degree in  $\gamma$  form, was directly plotted against temperature in Figure 3c. The intensity increase of  $1700\text{ cm}^{-1}$  band was firstly observed from room temperature up to about  $60\text{ }^{\circ}\text{C}$  reflecting the growth of  $\gamma$ -nanocrystals along the channels of MCM-41 matrix. The intensity decrease of the  $1700\text{ cm}^{-1}$  band, distinctive of the presence of  $\gamma$ -nanocrystals, is reflecting the equilibrium melting points (ranging from  $60\text{ }^{\circ}\text{C}$  up to  $90\text{ }^{\circ}\text{C}$ ) of a broad size distribution of nanocrystals within the pores with respect to  $T_m = 161\text{ }^{\circ}\text{C}$ [22] for  $\gamma$ -crystals, according to the Gibbs-Thomson equation. It is worth noting that the signal of the  $1700\text{ cm}^{-1}$  band distinctive of  $\gamma$ -crystals is no longer detectable above  $90\text{ }^{\circ}\text{C}$ , confirming the absence of IMC outside the pores and the complete loading of IMC. Figure 3a clearly shows that the intensity of the  $1700\text{ cm}^{-1}$  band increases to the detriment of the band centered at  $1680\text{ cm}^{-1}$  during the growth of  $\gamma$ -nanocrystals, while during the melting of nanocrystals the intensity of the  $1700\text{ cm}^{-1}$  band decreases in favor of a broad component centered around  $1660\text{ cm}^{-1}$ .

It is worth mentioning that upon a second heating under the same conditions as the first heating no recrystallization was detected (Figure 3b), indicating that the crystal growth from preexisting  $\gamma$ -nuclei in the freshly-prepared composite. This is also consistent with the value of the Avrami exponent close to 1, interpreted as reflecting the 1-dimensional growth and the bypass nucleation. It is also the demonstration that the phase transformations of IMC under confinement described in this paper are only possible by using MAL method.

Spectra of the composite collected at room temperature at the end of the isothermal transformation and after a first heating are superimposed, and compared in Figure 4 to those of the freshly prepared composite and amorphous IMC in the bulk form. A special attention is given to the  $1650 - 1750\text{ cm}^{-1}$  region in the C=O stretching spectrum, since Figure 1 and previous analyzes[18, 23, 24] have clearly shown that the amorphous and polymorphism can be undoubtedly identified in this region. In the bulk form, the broad  $1680\text{ cm}^{-1}$  band and the sharp  $1700\text{ cm}^{-1}$  band correspond to disordered and ordered arrangements of IMC dimers in the amorphous and  $\gamma$ -crystalline states respectively. It is clearly observed that the bandshape of the amorphous state taken at the end of isothermal or non-isothermal transformation is different from the bandshape of the spectrum of the bulk form of amorphous IMC obtained by quenching the liquid. This indicates an isothermal or non-isothermal transformation of the original amorphous form A1 (distinctive of the bulk form) towards a second new amorphous form A2 via nanocrystallization, only observed under confinement.

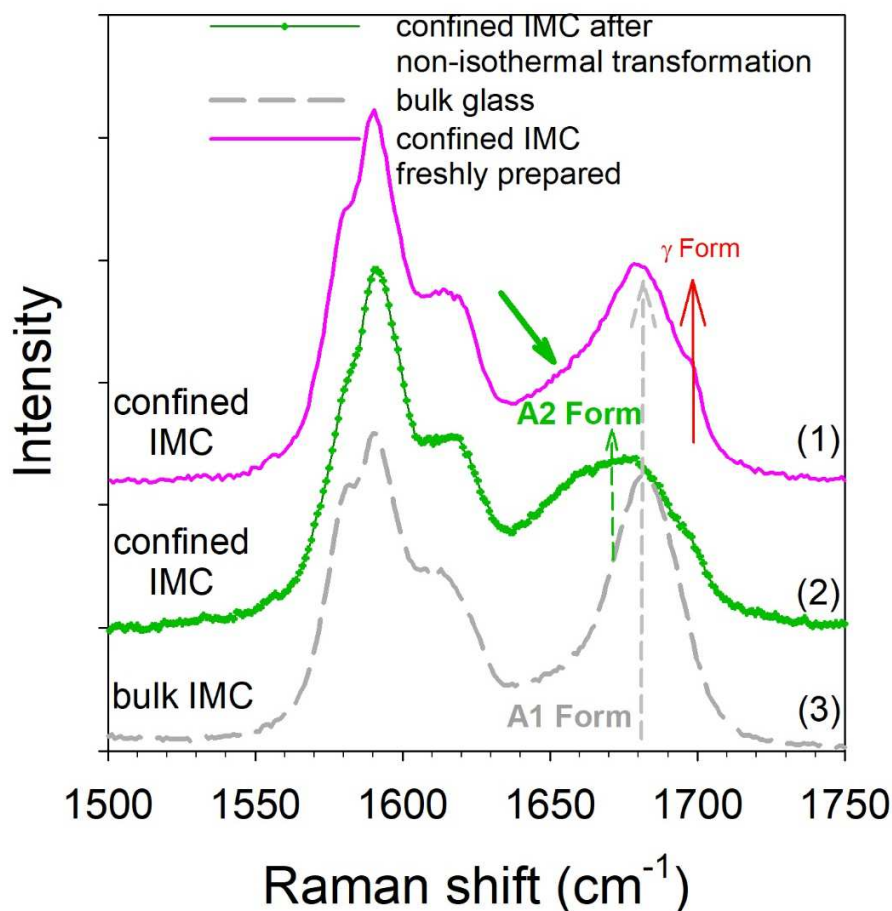


Figure 4. Comparison at room temperature of amorphous IMC forms, in bulk (3) and confined in MCM-41 matrix at 20% of IMC, collected directly on a freshly prepared composite (1), after a first heating of the freshly prepared composite (2) up to 120 °C (temperature above the complete melting of nanocrystals. Bulk IMC (3) was obtained by quenching the liquid. Spectra are shifted along Y-axis for better clarity. The vertical arrows indicate the intensity maximum of the bands distinctive of the dimer organization in the A1 form (dashed thick line), in the A2 form (dashed thin line) and in  $\gamma$ -crystals. The arrow (thick line) in spectrum (1) highlights a tail resulting from a minor contribution of A2 form

The C=O stretching spectrum of the freshly prepared composite (spectrum (1) in Figure 4) shows the coexistence of two different amorphous forms with a weak contribution of  $\gamma$ -nanocrystals at the early stage of the isothermal annealing. (i) The amorphous form distinctive of the bulk (A1) corresponding to Raman intensity centered around 1680  $\text{cm}^{-1}$  which decreases upon annealing (Fig. 3a) to the detriment to the 1700  $\text{cm}^{-1}$  band, signature of  $\gamma$ -crystallites. It can be observed in Figure 3a that the melting of  $\gamma$ -crystallites gives a contribution to the spectrum at wavenumbers lower than 1680  $\text{cm}^{-1}$ , corresponding to the signature of a second amorphous form. (ii) The second amorphous form (A2) can be identified by a broad band centered around 1660  $\text{cm}^{-1}$ , much broader than the 1680  $\text{cm}^{-1}$  band distinctive of the A1 form. After melting of nanocrystals upon heating or after isothermal transformation under a long annealing, the spectrum (2) in Figure 4 is clearly different from the spectrum (3) of A1 form, especially between 1640 and 1750  $\text{cm}^{-1}$ . This clearly indicates that form A1 transforms into form A2 via nanocrystallization.

**Low-wavenumber Raman** spectra of the two amorphous forms were firstly collected at room temperature. Form A1 was obtained after quenching the liquid state in the bulk form, while form A2 was obtained after a first heating of the composite from -50 °C up to 120°C instantaneously cooled down to room temperature. Using data processing described in Figure S6 and widely described in previous papers[20, 25-27] Raman intensity was firstly converted into reduced intensity ( $I_r(\omega)$  plotted in Figure 5a) and then in Raman susceptibility ( $\chi''(\omega)$ , in Figure 5b) exclusively resulting from the vibrational component of the low-wavenumber intensity. The reduced intensity representation promotes the observation of rapid relaxational motions characterized by a Lorentzian shape. Spectra collected on the composite during two successive heating ramps are plotted in Figures S7a and S7b. The low-wavenumber spectra collected during the first heating ramp of the composite reveal the presence of phonon peaks rigorously corresponding to those of  $\gamma$ -crystals in the bulk form, reflecting unambiguously the growth and melting of  $\gamma$ -nanocrystals upon heating (see Figure S7c). In molecular liquids the temperature dependence of the Lorentzian intensity associated to the quasielastic intensity is empirically recognized as inversely proportional to that of the logarithm of the dynamical viscosity[20, 28] and can be used for highlighting order-disorder phase transitions, including the detection of the glass transition. The Raman susceptibility was considered as a representation close to the vibrational density of states usually obtained by inelastic neutron scattering[29], and can be used for comparing the molecular organization in both amorphous states.  $I_r(\omega)$  and  $\chi''(\omega)$  spectra of A1 (bulk) and A2 amorphous forms in the  $\gamma$ -IMC(20%):MCM-41 composite are plotted in Figures 5a and 5b respectively. Both types of representations of the low-wavenumber spectra are different demonstrating a difference between molecular mobility and molecular organization in the two amorphous states. The temperature dependence of the quasielastic intensity can be obtained by integration of the Lorentzian component and was plotted for A1 (bulk) and A2 (confined) amorphous forms in Figure 5c.  $T_g$  is detected around 40 °C via a break in  $I_{QES}(T)$  in the A1 (bulk) form as expected from the literature[16], and around 10 °C in the A2 form reflecting a higher molecular mobility than in the bulk form (A1). Consequently, the amorphous form A2 only existing under confinement is characterized by a higher mobility than that of the original amorphous bulk form. It is interesting to note that  $I_{QES}(T)$  obtained in the first heating of the composite is quasi superimposed with data of the bulk form up to  $T_g$  of A1 form (~ 40 °C), and becomes superimposed with data of the 2<sup>nd</sup> heating ramp above 60 °C. The change observed at 40 °C can be obviously interpreted as the glass transition of A1 form, since Figures 1 and 4 show that the main contribution of the spectrum (above 1650  $\text{cm}^{-1}$ ) of the freshly prepared composite corresponds to the contribution of the A1 form (1680  $\text{cm}^{-1}$  band). The temperature dependence of the intensity of the phonon peak located at 70  $\text{cm}^{-1}$  (see Fig. S7) is compared the  $I_{QES}(T)$  plot in Figure 5d. It is observed that  $\gamma$ -nanocrystals begin to melt just above  $T_g$  of the A1 form composed of  $\gamma$ -nuclei, and the change in  $I_{QES}(T)$  observed between 40 and 60 °C results from the glass transition of A1 form and the melting of nanocrystals into form A2. Consequently, both investigations in the C=O stretching region and in the low-wavenumber range converge into the description of a transformation of confined A1 form into  $\gamma$ -nanocrystals which melt into A2 form.

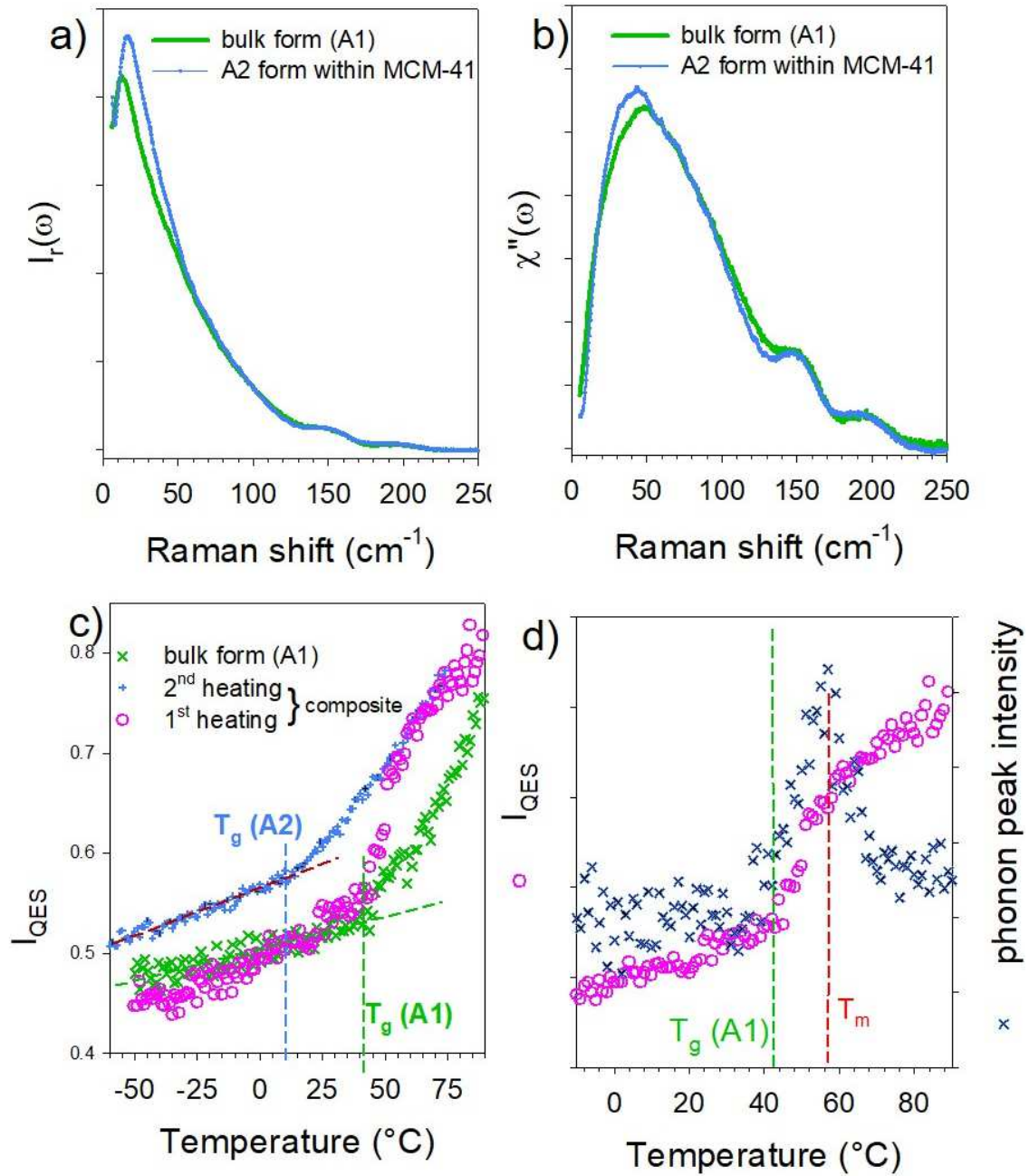


Figure 5. Low-wavenumber spectra of A1 (bulk form) and A2 (confined) amorphous forms; a) spectra represented in the reduced intensity; b) Raman susceptibility representation; c) temperature dependence of the quasielastic intensity obtained from spectra collected upon heating bulk amorphous form (A1), upon a first heating of the freshly prepared composite and a second consecutive heating of the composite performed directly after cooling; d)  $I_{\text{QES}}(T)$  is compared with the time dependence of the intensity of the phonon peak located at  $70 \text{ cm}^{-1}$

While the melting of  $\gamma$ -IMC inside pores nanocrystals upon heating can be explained by the Gibbs-Thomson effect, the observation of nanocrystal instability in the continuity of the

isothermal growth is a very original phenomenon. The stability of nanocrystals can be understood from specific consideration on the surface term in the Gibbs energy. It was shown[10] that the equilibrium size of a nanocrystal is controlled by the specific area rather than the surface curvature. Under geometrical confinement, the specific area is greatly imposed by the geometry of the MCM-41 matrices, i.e. by the curvature radius of cylindrical channels. At room temperature the growth rate of IMC crystals can be limited by interfacial effects which become preponderant with respect to thermal energy. In this case, the high specific area of nanocrystals achieved upon the 1-dimensional growth makes them thermodynamically unstable. As a consequence, IMC  $\gamma$ -nanocrystals could slowly dissolve in the coexisting second amorphous liquid (A2), since they become more soluble in a less viscous A2 liquid form. This very slow transformation of  $\gamma$ -nanocrystals into A2 amorphous form can be identified as a digestive ripening corresponding to the inverse Ostwald ripening, used for preparing monodisperse nanocrystals of different metals and still considered as puzzling mechanism [30].

#### 4. Conclusion

Using MAL method for loading molecular materials within MCM-41 gives the opportunity to explore new routes of manipulating matter and to analyze original transformation of physical states. No crystallization of pharmaceuticals was previously observed in MCM-41 or SBA-15 matrices by using classical methods of loading based on capillarity[31], while confinement within pores of larger size ( $\geq 7nm$ ) gives a nice opportunity to stabilize various polymorphic nanocrystalline forms[32]. By selecting indomethacin, characterized by  $T_g = 42^\circ C$ , close to the temperature of loading (RT) and nearly corresponding to the maximum of nucleation and growth rates, original physical states and transformations of the confined matter were investigated. Indeed, the present study reveals a two-step transformation of the A1 amorphous form corresponding to the 1-dimensional growth of  $\gamma$ -nanocrystals from preexisting nuclei in the A1 form which transform into A2 form by a mechanism depending on the route (isothermal or non-isothermal). Upon heating nanocrystals become unstable because of Gibbs-Thomson effects and melt into A2 form. Upon annealing at room temperature, the instability of nanocrystals is resulting from a too large specific area imposed by the 1-dimensional growth along cylindrical pores, and they dissolve into A2 form by a mechanism similar to digestive ripening by which larger clusters (nanocrystals) dissolve transferring their mass to smaller ones (A2 form). The second amorphous form is characterized by a higher molecular mobility with  $T_g$  about 30 degrees lower than that of the original A1 form. The isothermal dissolution begins when the equilibrium size of  $\gamma$ -nanocrystals imposed by the geometry of MCM-41 matrices is reached. This study shows that this original phenomenon of crystal dissolution after crystallization is only possible after loading IMC at the solid-state in MCM-41 matrices with our innovative MAL method, imposing severe spatial restrictions. Previous investigations[33, 34] of IMC confined in MCM-41 have shown the coexistence of amorphous with nanocrystals of IMC and polymorphic transformations without certitude that crystallized IMC was really confined, given the very limited Gibbs-Thomson effect detected on the melting temperature. On the other hand, it was

shown that it was possible to prepare amorphous forms different from the bulk IMC by vapor deposition[35] or upon pressurization[36], characterized by high-density molecular packing. Under confinement a lower density of the molecular packing is expected according to previous studies showing that low-density of confined materials prevents crystallization. It was also previous shown that other confined APIs present amorphous forms different from the bulk form with higher mobility[12, 37-39]. However, no such isothermal two-step transformation towards an amorphous form via the growth of nanocrystals followed by dissolution was previously observed. The observation of this original two-step isothermal transformation shows that the pore size of MCM-41 is the crucial parameter making unstable nanocrystals in the course of their growth. This phenomenon was systematically observed by replicating the experiments for same composites and for composites prepared with various filling degrees, as shown in Figure S8.

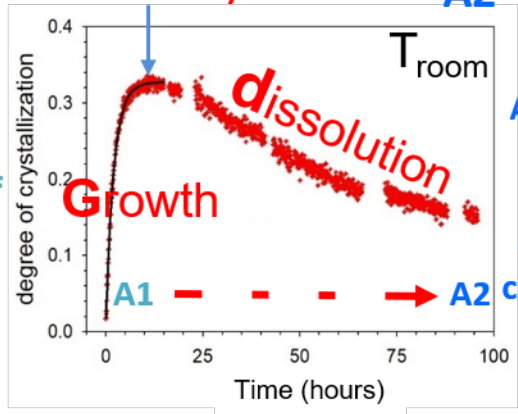
## References

- [1] I. Cohen, A. Ha, X. Zhao, M.F. Lee, T., M.J. Strouse, D. Kivelson, A low-temperature amorphous phase in a fragile glass-forming substance, *Journal of Physical Chemistry*, 100 (1996) 8518-8526.
- [2] B.V. Bolshakov, A.G. Dzhonson, On the Number of Amorphous Phases in n-Butanol, *Doklady Physical Chemistry*, 393 (2003) 318–320.
- [3] M. Zhu, L. Yu, Polyamorphism of D-mannitol, *J. Chem. Phys.*, 146 (2017) 244503.
- [4] O. Mishima, L.D. Calvert, E. Whalley, An apparently first-order transition between two amorphous phases of ice induced by pressure, *Nature*, 314 (1985) 76-78.
- [5] M. Kobayashi, H. Tanaka, The reversibility and first-order nature of liquid-liquid transition in a molecular liquid, *Nature Communications*, 7 (2016) 13438 13431-13438.
- [6] H. Tanaka, Liquid-liquid transition and polyamorphism, *J. Chem. Phys.*, 153 (2020) 130901-130943.
- [7] M. Beasley, B. Kasting, M. Tracy, A. Guiseppi-Elie, R. Richert, M. Ediger, Physical vapor deposition of a polyamorphic system: triphenyl phosphite, *J. Chem. Phys.*, 153 (2020) 124511.
- [8] A. Hédoux, Y. Guinet, P. Derollez, O. Hernandez, R. Lefort, M. Descamps, A contribution to the understanding of the polyamorphism situation in triphenyl phosphite, *Phys. Chem. Chem. Phys.*, 6 (2004) 3192-3199.
- [9] Y. Guinet, L. Paccou, A. Hédoux, A detailed description of the devitrification mechanism of D-mannitol, *Phys. Chem. Chem. Phys.*, 22 (2020) 5011-5017.
- [10] G. Kaptay, The Gibbs Equation versus the Kelvin and the Gibbs-Thomson Equations to Describe Nucleation and equilibrium of Nano-Materials, *J. Nanosci. Nanotechnol.*, 12 (2011) 1-9.
- [11] G. Madras, B. McCoy, Transition from nucleation and growth to Ostwald ripening, *Chem. Eng. Sci.*, 57 (2002) 3809-3818.
- [12] B. Malfait, N. Correia, A. Mussi, L. Paccou, Y. Guinet, A. Hédoux, Solid-state loading of organic molecular materials within mesoporous silica matrix: application to ibuprofen, *Micro. Meso. Mater.*, 277 (2019) 203-207.
- [13] B. Malfait, N. Correia, C. Ciotonea, J. Dhainaut, J.-P. Dacquin, S. Royer, N. Tabary, Y. Guinet, A. Hédoux, Manipulating the Physical states of confined ibuprofen in SBA-15 based drug delivery systems obtained by solid-state loading: impact of the loading degree, *J. Chem. Phys.*, 153 (2020) 154506-154513.
- [14] K. Trzeciak, S. Kazmierski, K. Druzbecki, M. Potrzebowski, Mapping of Guest Localization in Mesoporous Silica Particles by Solid-State NMR and Ab Initio Modeling: New Insights into Benzoic Acid and p-Fluorobenzoic Acid Embedded in MCM-41 via Ball Milling, *J. Phys. Chem. C*, 125 (2021) 10096-10109.
- [15] X. Chen, K.R. Morris, U.J. Griesser, S.R. Byrn, J.G. Stowell, Reactivity differences of indomethacin solid forms with ammonia gas, *Journal of the American Chemical Society*, 124 (2002) 15012-15019.
- [16] V. Andronis, G. Zografi, The molecular mobility of supercooled amorphous indomethacin as a function of temperature and relative humidity, *Pharmaceutical research*, 15 (1998) 835-842.
- [17] J.-F. Willart, M. Descamps, Solid State Amorphization of Pharmaceuticals, *Molecular Pharmaceutics*, 5 (2008) 905-920.
- [18] L.S. Taylor, G. Zografi, Spectroscopic characterization of interactions between PVP and indomethacin in amorphous molecular dispersions, *Pharmaceutical research*, 14 (1997) 1691-1698.
- [19] L.S. Taylor, G. Zografi, The quantitative analysis of crystallinity using FT-Raman spectroscopy, *Pharmaceutical research*, 15 (1998) 755-761.
- [20] A. Hédoux, Recent developments in the Raman and infrared investigations of amorphous pharmaceuticals and protein formulations: a review, *Adv. Drug Deliv. Rev.*, 100 (2016) 133-146.
- [21] H.-J. Jou, M.T. Lusk, Comparison of Johnson-Mehl-Avrami-Kolmogorov kinetics with a phase-field model for microstructural evolution driven by substructure energy, *Physical Review B*, 55 (1997) 8114-8121.

- [22] V. Andronis, G. Zografi, Crystal nucleation and growth of indomethacin polymorphs from the amorphous state, *Journal of Non Crystalline Solids*, 271 (2000) 236-248.
- [23] A.G. Schmidt, S. Wartewig, K.M. Picker, Polyethylene oxides: protection potential against polymorphic transitions of drugs?, *Journal of Raman Spectroscopy*, 35 (2004) 360-367.
- [24] A. Hédoux, L. Paccou, Y. Guinet, J.-F. Willart, M. Descamps, Using the low-frequency Raman spectroscopy to analyze the crystallization of amorphous indomethacin, *European Journal of Pharmaceutical Sciences*, 38 (2009) 156-164.
- [25] A. Hédoux, Y. Guinet, M. Descamps, The contribution of Raman spectroscopy to the analysis of phase transformations in pharmaceutical compounds, *Int. J. Pharm.*, 417 (2011) 17-31.
- [26] Y. Guinet, L. Paccou, F. Danede, J.F. Willart, P. Derollez, A. Hédoux, Comparison of amorphous states prepared by melt-quenching and cryomilling polymorphs of carbamazépine, *Int. J. Pharm.*, 509 (2016) 305-313.
- [27] B. Malfait, L. Paccou, P. derollez, Y. Guinet, A. Hedoux, Capabilities of low-wavenumber Raman spectroscopy for analyzing the mechanism of devitrification of molecular glasses, *J. Raman Spectr.*, 50 (2019) 1027-1033.
- [28] M.C.C. Ribeiro, Low-frequency Raman spectra and fragility of imidazolium ionic liquids, *J. Chem. Phys.*, 133 (2010) 24503-24506.
- [29] A. Hedoux, P. Derollez, Y. Guinet, A.J. Dianoux, M. Descamps, Low-frequency vibrational excitations in the amorphous and crystalline states of triphenyl phosphite: A neutron and Raman scattering investigation - art. no. 144202, *Physical Review B*, 63 (2001) 144202.
- [30] J. Shimpi, D. Sidhaye, B. Prasad, Digestive Ripening: A Fine Chemical Machining Process on the Nanoscale, *Langmuir*, 33 (2017) 9491-9507.
- [31] K. Nartowski, D. Malhotra, L. Hawarden, J. Sibik, D. Iuga, J.A. Zeitler, L. Fabian, Z. Khimyak, F NMR Spectroscopy as a Highly Sensitive Method for the Direct Monitoring of Confined Crystallization within Nanoporous Materials, *Angew. Chem. Int. Ed.*, 55 (2016) 8904-8908.
- [32] M. Beinier, G. Rengarajan, S. Pankaj, D. Enke, M. Steinhart, Manipulating the crystalline state of pharmaceuticals by nanoconfinement, *Nano Lett.*, 7 (2007) 1381-1385.
- [33] S. Hellsten, H. Qu, T. Heikkila, J. Kohonen, S. Reinikainen, Raman spectroscopic imaging of indomethacin loaded in porous silica, *CrystEngComm*, 14 (2012) 1582-1587.
- [34] T. Ukmar, A. Godec, O. Planinsek, V. Kaucic, G. Mali, M. Gaberscek, The phase (trans)formation and physical state of a model drug in mesoscopic confinement, *Phys. Chem. Chem. Phys.*, 13 (2011) 16046-16054.
- [35] S. Shakeel, M. Ediger, Molecular Orientation in Stable Glasses of Indomethacin, *J. Phys. Chem. Lett.*, 3 (2012) 1229-1233.
- [36] A. Hedoux, Y. Guinet, F. Capet, L. Paccou, M. Descamps, Evidence for a high-density amorphous form in indomethacin from Raman scattering investigations, *Phys. Rev. B*, 77 (2008) 094205-094201-094210.
- [37] C. Jackson, G. McKenna, The glass transition of organic liquids confined to small pores, *J. Non-Cryst. Sol.*, 131-133 (1991) 221-224.
- [38] R. Richert, Dynamics of nanoconfined supercooled liquids, *Annu. Rev. Phys. Chem.*, 62 (2011) 65-84.
- [39] W. Thompson, Perspective: Dynamics of confined liquids, *J. Chem. Phys.*, 149 (2018) 170901.



Amorphous form distinctive of the bulk



Amorphous form detected only under confinement